biology

MDPI

*Article*

# In silico prediction of phosphorylation of NS3 as an essential mechanism for Dengue virus replication and the antiviral activity of Quercetin

**Lamya Alomair [1], Fahad Almsned [2], Aman Ullah [3] and Mohsin S. Jafri [4,*]**

[1] School of Systems Biology and the Krasnow Institute for Advanced Study, George Mason University, Fairfax VA 22030, USA; and King Abdullah International Medical Research Center, Riyadh, Kingdom of Saudi Arabia; OmairL@NGHA.MED.SA
[2] School of Systems Biology and the Krasnow Institute for Advanced Study, George Mason University, Fairfax VA 22030, USA and King Fahad Specialist Hospital – Dammam, Dammam, Kingdom of Saudi Arabia; Fahad Almsned <falmsned@masonlive.gmu.edu>
[3] School of Systems Biology and the Krasnow Institute for Advanced Study, George Mason University, Fairfax VA 22030, USA; e-mail@e-mail.com
[4] School of Systems Biology and the Krasnow Institute for Advanced Study, George Mason University, Fairfax VA 22030, USA and Center for Biomedical Engineering and Technology, University of Maryland School of Medicine, Baltimore MD 21201, USA; sjafri@gmu.edu

* Correspondence: sjafri@gmu.edu; Tel.: +1 703-993-8420

**Simple Summary:** Dengue is a mosquito-borne virus that infects up to 400 million people worldwide annually. Dengue infection triggers high fever, severe body aches, rash, low platelet count, and could lead to Dengue Hemorrhagic Fever (DHF) in some cases. There is currently no cure nor a broadly effective vaccine. The interaction of two viral proteins, NS3 and NS5 (Nonstructural Proteins 3 and 5), is required for viral replication in the infected host's cells. Our computational modeling of NS3 suggested that phosphorylation of a serine residue at position 137 of NS3 by a specific c-Jun N-terminal kinase (JNK) enhances viral replication by increasing the interaction of NS3 and NS5 through structural changes in amino acid residues 49-95. Experimental studies have shown that inhibition of JNK prevents viral replication and have suggested that the plants' flavonoid Quercetin, Agathis flavone, and Myricetin inhibit Dengue infection. Our molecular simulations revealed that Quercetin binds NS3 and obstruct serine 137 phosphorylation, which may decrease viral replication. This work offers a molecular mechanism that can be used for anti-Dengue drug development.

**Citation:** Alomair, L.; Almsned, F.; Ullah, A.; Jafri, M. In silico prediction of phosphorylation of NS3 as an essential mechanism for Dengue virus replication and the antiviral activity of Quercetin . *Biology* **2021**, *10*, x. https://doi.org/10.3390/xxxxx

Academic Editor: Firstname Lastname
Received: date
Accepted: date
Published: date



**Abstract:** Dengue virus infection is a global health problem for which there have been challenges to obtaining a cure. Current vaccines and anti-viral drugs can only be narrowly applied in ongoing clinical trials. We employed computational methods based on structure-function relationships between human host kinases and viral Nonstructural Protein 3 (NS3) to understand viral replication inhibitors' therapeutic effect. Phosphorylation at each of the two most evolutionarily conserved sites of NS3, serine 137 and threonine 189, compared to the unphosphorylated state were studied with molecular dynamics and docking simulations. The simulations suggested that phosphorylation at serine 137 caused a more remarkable structural change than phosphorylation at threonine 189, specifically located at amino acid residues 49-95. Docking studies supported the idea that phosphorylation at serine 137 increased the binding affinity between NS3 and Nonstructural Protein 5 (NS5), whereas phosphorylation at threonine 189 decreased it. The interaction between NS3 and NS5 is essential for viral replication. Docking studies with the antiviral plant flavonoid Quercetin with NS3 indicated that Quercetin physically occluded the serine 137 phosphorylation site. Taken together, these findings suggested a specific site and mechanism by which Quercetin inhibits dengue and possible other flaviviruses.

**Keywords:** dengue, NS3, phosphorylation, quercetin

## 1. Introduction

Dengue virus (DENV), also is known as break-bone fever, is a global health concern afflicting around 400 million individuals in more than 100 countries [1,2]. DENV causes severe illness, and sometimes, a potentially deadly complication called Dengue Hemorrhagic Fever (DHF) [3,4]. The prevalence of Dengue fever has grown dramatically worldwide in recent decades. Dengue's global spread poses a severe health threat because there are neither specific drugs to treat nor a broadly effective vaccine to prevent Dengue infection [5-12]. Recent studies indicated that the plant flavonoids Quercetin, Agathisflavone, and Myricetin inhibit Dengue infection and bind to the same specific site of the viral Nonstructural Protein 3 (NS3) [13,14]. However, the exact mechanism for this inhibition remains unclear. In this study, we performed a bioinformatic analysis of the Dengue Proteome to identify amino acid modifications by kinases that are likely to affect viral interaction partners in the human host. We then used molecular simulation to test the functional consequences of phosphorylation at specific sites in NS3. Finally, we studied the predicted binding site for the antiviral drug Quercetin to increase understanding of it mode of action.

The DENV genome encodes a polyprotein of 3391 amino acid residues with a gene order of 5′-C-prM-E-NS1-NS2A-NS2B-NS3-NS4A-NS4B-NS5-3′, ten viral proteins, including three structural proteins, and seven nonstructural [15]. The structural proteins are responsible for virion formation. In contrast, the nonstructural proteins play roles in the synthesis of viral RNA replication [16]. The viral proteins such as Nonstructural Protein 3 (NS3) and Nonstructural Protein 5 (NS5) that take part in viral replication and viral protein synthesis enter the host cell and migrate to the Endoplasmic Reticulum (ER) membrane, which is the site of protein synthesis in the host cell, to use cellular pathways for viral replication [17-19]. DENV is a member of the Flaviviridae family that includes the West Nile virus (WNV), yellow fever virus, Zika virus, and Hepatitis C virus (HCV). NS3 shares a high degree of homology with other members of this family, as shown in the amino acid multiple sequence alignment in Supplemental Fig. S2 [20-24]. The relationship of members in this family based on this alignment is shown in Fig. S3.

Both NS3 and NS5 are viral proteins that are vital components in DENV replication. Additionally, NS3 and NS5 contain conserved motifs found in several RNA helicases and RNA-dependent RNA polymerases, respectively [25]. Phosphorylation of NS5 is critical to its function and association with NS3. Prior research has supported a mechanism where the phosphorylation state of NS5 controls the association/disassociation of NS3 with NS5, which affects viral replication [26]. NS3 is the second-largest key component in DENV replication machinery. The multifunctional enzyme NS3 performs various viral replication actions and plays an essential role in antiviral evasion [27]. However, there is a gap in our understanding of the role of NS3 in molecular mechanisms underlying the replication of DENV.

Our lab recently used a computational approach, which predicted that NS3 could be phosphorylated by around 500 human kinases [28]. We hypothesized that inhibition of kinases responsible for phosphorylation might inhibit viral replication. We predicted the kinases that are most likely to phosphorylate NS3 by using neural networks and other machine learning algorithms to calculate and rank the score of top kinases that phosphorylate DENV NS3 [28]. We applied a range of computational methods, including molecular simulations, to classify the functional impact or phosphorylation of NS3 structure on viral replication at the molecular level. This paper explores the structural effects caused by NS3 amino acid residue phosphorylation at the two sites, serine 137 (S137) and threonine 189 (T189) and the potential impact of these structural effects on

NS3 and NS5 interaction, and consequently, on DENV viral replication. These two proteins were chosen for study because NS3 and NS5 are considered to be promising drug targets [22]. Lastly, we predicted a mechanism behind the anti-viral Quercetin action through its interaction with NS3.

## 2. Materials and Methods

The molecular dynamics trajectories and the supporting files are available in the Mason Archival Repository Service (MARS): https://doi.org/10.13021/dwk3-ys70

### 2.1. *Predicting phosphorylation.*

To investigate possible amino acids that might be phosphorylated by human kinases, we analyzed the NS3 amino acid sequence by three online tools: GPS 3.0 (http://gps.biocuckoo.org/online.php), NetPhos 3.1 (http://www.cbs.dtu.dk/services/NetPhos/), and Scansite 3 (https://scansite4.mit.edu/), which were listed in a recent study as among the most reliable phospho-algorithms [29-32]. The candidates were ranked using a combination of the highest scores and a site being found by all three tools. The 20 top candidate sites were compared using multiple sequence alignment (MSA) across the NS3 dengue virus sequences for sequence conservation. The most conserved predicted phosphorylated sites (S137 and T189) were chosen for further study by molecular simulation.

### 2.2 *System Preparation for Molecular Simulation*

#### *2.2.1.* Initial structure

We retrieved the initial NS3 structure (PDB: 2VBC) from the Protein Data Bank (PDB) obtained from the crystallized structure [33,34] (Fig. 1A). The initial structure has been visualized and processed using UCSF Chimera (v 1.14). Structures were viewed using Visual Molecular Dynamics viewer (VMD v1.9.3) [35].

#### 2.2.2 Phosphorylated structure

Since NS3 phosphorylation at serine 137 and threonine 189 was our study's focus, we used the Visual Molecular Dynamics viewer (VMD, v1.9.3) to generate two NS3 phosphorylated systems; S137 and T189. S137 was generated using SP2 phosphoserine patch and T189 using THP2 phosphothreonine patch. The phosphorylation patches were saved in the Supplemental files as "psfgen_phosphorlation137.pgn" and "psfgen_phosphorlation189.pgn".

#### 2.2.3. Solvation

The three NS3 structures (the unphosphorylated NS3 (WT), S137, and T189) were solvated in a cubic periodic box with a three-site transferrable intermolecular potential (TIP3P) water model with minimum distance from the protein surface using VMD [36]. The wild-type system had 36163 atoms (9517 molecular atoms and 26646 water molecules). Each phosphorylated protein system had 36166 atoms (9520 molecular atoms and 26646 water molecules).

#### 2.2.4. Simulations Steps

The Molecular Dynamics (MD) Simulation was prepared and run by Nanoscale Molecular Dynamics (NAMD 2.13 for Win64-multicore-CUDA) with the CHARMM36 all-force field parameters parallel programming model [37,38]. Periodic boundary conditions were applied, and structures were reported every picosecond (ps). We used a 12 Å cutoff for Van Der Waals interaction with a switching function distance of 8 Å, and the smooth particle-mesh Ewald (PME) method was enabled accordingly. Before the MD simulation, all the flowing procedures were applied to all three systems.

#### 2.2.5. Minimization

Each system was energetically minimized to relax possible steric clashes and obtain a low energy start conformation. A total of 2000 steps of minimization were performed.

We used the NAMD script "2VBC_wb_equil.namd", which is included as supplemental material, to perform this step.

2.2.6. Heating

Each system was heated from 273 K to the average physiological temperature (300 K) for 300 ps. The Langevin thermostat was applied. The temperature was incremented slowly by 0.001K. We used the NAMD script "2VBC_wb_heat.amd", which is included as supplemental material, to perform this step.

2.2.7. Equilibration

Each system was equilibrated to adjust the system density under Isothermal–isobaric (NPT) ensemble conditions for 200 ps. We used the NAMD script "2VBC_wb_min.namd", which is included as supplemental material, to perform this step.

2.2.8. MD Simulation

Each system was then MD simulated to sample the structural characteristics and dynamics at 300K using Microcanonical ensemble (NVE) for 100 nanoseconds (ns) under Isothermal–isobaric (NPT) ensemble and with a time step of 1 femtosecond (fs). The long-range electrostatics was handled using the particle-mesh Ewald (PME) method [39]. The atom coordinates were recorded every 1 ps throughout the simulation. Moreover, 1 fs integration step was used for all simulations. We used the NAMD script "2VBC_wb_quench.namd", which is included as supplemental material, to perform this step.

2.2.9. Trajectories Analysis

The Root Means Square Deviation (RMSD), Root Mean Square Fluctuation (RMSF), and Principal Component Analysis (PCA) were calculated for all trajectory structures using the Bio3D R package (v 2.4-1) [40,41]. Hierarchical Cluster analysis of the scaled Ψ and Φ was conducted using stats R package (v 3.6.2) (https://www.rdocumentation.org/packages/stats/versions/3.6.2). The RMSD, RMSF, Ramachandran (Ψ and Φ angles), PCA, and Hierarchical Clustering plots were generated using the ggplot2 R package (v 3.3.2) (https://ggplot2.tidyverse.org/authors.html) and the ggpubr R package (v 0.4.0) (https://cran.r-project.org/web/packages/ggpubr/index.html). We used the dplyr (v 1.0.2) (https://cran.r-project.org/web/packages/dplyr/index.html) and the tidyverse R package (v 1.3.0) (https://cran.r-project.org/web/packages/dplyr/index.html ) for data manipulation. The Analysis of Covariance (ANCOVA) was used to analyze the significance between RMSD means for the three simulated structures (unphosphorylated WT at time 100 ns, S137 at time 100 ns, and T189 at time 100 ns) while correcting for the within-structures time steps variability using the rstatix R package (v 0.6.0) (https://cran.r-project.org/web/packages/rstatix/index.html). Post-hoc pairwise comparisons of estimated marginal means (adjusted means) were performed to identify which pairs are different using the emmeans R package (v 1.5.3) (https://cran.r-project.org/web/packages/emmeans/index.html). The Bonferroni multiple testing correction is applied [42]

2.2.10. Docking

The 3D structures of interacting proteins can provide valuable atomic level information regarding the protein-protein interface details. We used ClusPro 2.0, a protein-protein docking algorithm server, to evaluate the docking of WT, S137, and T189 against NS5. [43-45]. The MD simulation frame were used for each of the three dockings at time 100 ns atomic coordinates against NS5 (PDB: 2J7U). The docking of Quercetin (PubChem CID: 5280343) was performed against the protease domain of NS3 (PDB: 2VBC) using Autodock Vina (v 2.0) [46]. The Python scripts in the PyRx Virtual Screening software (v 0.9.8) were used to analyze the docking results [47]. UCSF Chimera (v 1.14) provided for interactive visualization and analysis of molecular structures [48].

## 3. Results

I*n silico* studies combined phosphorylation site prediction algorithms (GPS 3.0, NetPhos3.1, and Scansite3) followed by MD simulations were applied to assess the proteins (WT, S137, and T189) physical behavior [49,50]**.** Lastly, we used a protein-protein docking to evaluate phosphorylation's effect on the docking against NS5.

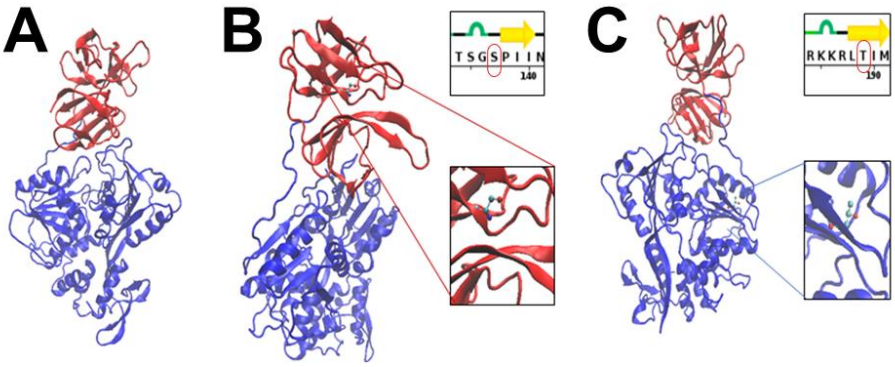


**Fig. 1 NS3 crystal structure.** (A) Crystal structure of the NS3 Protease-Helicase from Dengue virus (PDB:2VBC). The Protease domain (N-terminal, residues 20-168) is shown in red. The Helicase domain (C-terminal, NS3Hel, residues 180-618) is shown in blue. (B) Serine 137 residue (S137) location (cyan in inset) in NS3 conformation and its position in the amino acid sequence (circled in red). (C) Threonine 189 residue (T189) location (cyan in inset) in NS3 conformation and its position in the amino acid sequence (circled in red).

### 3.1 *Phosphorylation sites prediction*

The investigation of possible protein phosphorylation sites revealed many potential candidate positions on NS3 and several corresponding human kinases by all three algorithms (GPS 3.0, NetPhos3.1, and Scansite3), along with their score and residue position in the sequence. Identifying the top kinases required a three-tiered approach. In the first tier, we used the three phosphorylation site prediction tools, which suggested a total of 1489, 953, and 108 possible phosphorylation sites with the associated phosphorylating kinases, respectively. In many cases a particular site was predicted to be phosphorylated by multiple kinases. In the second tier, we considered in descending order kinases that have a combination of a high score along with a hit in each of the three tools. The number of kinases decreased to 61, 76, and 64, respectively, from the three tools listed above. In the third tier, we took the top 20 kinases from the list in the second tier (Supplemental Table S1). Evolutionarily, phosphoproteins are subject to more sequence conservation than their non-phosphorylated counterparts [51,52]. Hence, a Multiple Sequence Alignment (MSA) using Jalview (www.jalview.org) was applied to identify the most conserved regions among NS3 dengue virus sequences [53].

The two most evolutionarily conserved candidate sites on NS3 are serine 137 (S137), which was predicted to be phosphorylated by MAPK, GSK3, CDK1, or, and the residue threonine 189 (T189), which was predicted to be phosphorylated by Kinase AKT, PKB(AKT), or CAMK2G. NS3 contains an N-terminal protease domain (residues

19-168) and a C-terminal (residues 180-618) helicase domain and linker (residue 169-179) (Fig. 1). Both domains have been reported to have enzymatic activity and to be involved in NS3-NS5 interaction [54,55]. We examined the structural effects of phosphorylating one amino acid residue from each domain to gain insight into phosphorylation's role in both domains. A graphical representation of DENV NS3 (PDB: 2VBC) and the two sites (S137 and T189) is presented in Fig. 1. The domain (N-terminal) of the NS3 (residues 19-168) shown in red, the Linker (residues 169-179) shown in red, and the Helicase Domain (C-terminal) of NS3 (NS3Hel, residues 180-618) are shown in blue. In Fig. 1B, the S137 residue, shown in red (main panel and cyan in inset), can be found in the N-terminal domain. In Fig.1C, the T189 residue, shown in blue (main panel and cyan in inset), can be found in the C-terminal domain.

### *3.2. Effects of NS3 phosphorylation and conformational change in protein structure*

We examined the three NS3 structures (WT, S137, and T189) behavior under normal physiological conditions using MD simulation. The three simulations were performed for 100 ns at 300 K. Periodic boundary conditions were used with structures reported every 1 ps to study the phosphorylation's structural effects on NS3 structures.

Fig. 2 shows a Ramachandran plot and marginal density plot of all Ψ/Φ angles in four PDB structures: 1) unphosphorylated WT at time 0 ns, 2) unphosphorylated WT at time 100 ns, 3) S137 at time 100 ns, 4) T189 at time 100 ns (Fig. 2A). When using all Ψ/Φ angles, the four structures show a close pattern suggesting overall structure preservation with no significant conformational change than the original protein (unphosphorylated WT at time 0). The hierarchical clustering results for all Ψ angles showed the simulated structures' (unphosphorylated WT at time 100 ns, S137 at time 100 ns, and T189 at time 100 ns) tendency cluster together (Fig. 2B). Interestingly, the hierarchical clustering results for all Φ angles showed the tendency of unphosphorylated WT at time 0, unphosphorylated WT at time 100 ns, and T189 at time 100 ns cluster together that suggested a significant conformational change in S137 at time 100 ns (Fig. 2C).

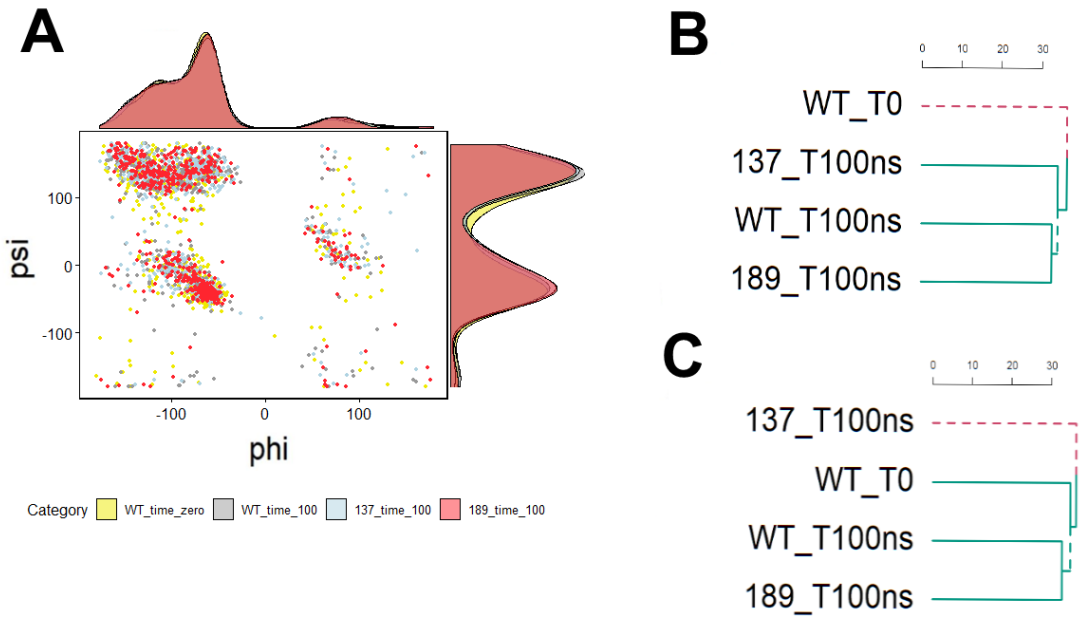


**Fig. 2 Ramachandran plot of NS3 backbone angles.** (A) The Ramachandran and density plots for all Ψ/Φ backbone angles for unphosphorylated WT at time 0 (yellow), unphosphorylated WT at time 100 ns (gray), S137 at time 100 ns (light blue), and T189 at

time 100 ns (light red). (B) Hierarchical clustering plot of all Ψ angles (C) Hierarchical clustering plot of all Φ angles.

We tracked the RMSD of all residues for the three MD simulated structures (unphosphorylated WT at time 100 ns, S137 at time 100 ns, and T189 at time 100 ns) throughout the simulation compared to the starting confirmation (unphosphorylated WT at time 0 ns) to measure the effect of phosphorylation of serine 137 and threonine 189 on the NS3 protein behavior (Fig. 3). The residues simulation showed a clear separation between the three simulated structures at time 100 ns (Fig. 3A). S137 had the highest RMSD, followed by WT. T189 had the lowest RMSD compared to the other two simulated structures. The same pattern is reflected in the three simulated structures' RMSD density plots (Fig. 3B). After adjustment for the simulation time steps, there was a statistically significant difference in all restudies RMSD between the groups, $F(2, 9590) = 59671.861$, $p < 0.0001$ (Table 1). We repeated the RMSD tracking for NS3 residues 49 to 94 only. S137 had the highest RMSD to both T189 and WT, which showed very close RMSD fluctuations throughout the simulation (Fig. 3C). RMSD density plots showed a clear separation of S137 from T189 and WT (Fig. 3D). After adjustment for the simulation time steps, there was a statistically significant difference in The (49 – 94) residues RMSD between the groups $F(2, 9590) = 1296396$, $p < 0.0001$ (Table 3). The RMSD score was statistically significantly greater in S137 (11.002 +/- 0.0045) compared to T189 (1.908+/- 0.0045) and WT (1.733 +/- 0.0045), $p < 0.001$ (Table 4).

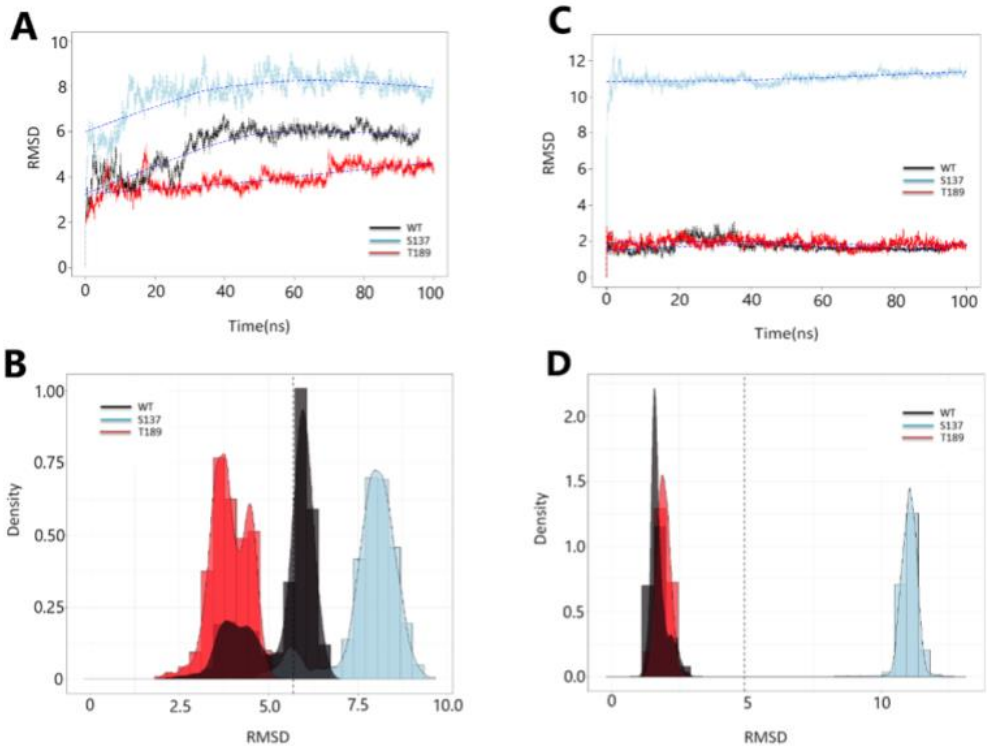

**Fig. 3 Root Mean Square Deviation (RMSD) Vs. MD simulation time and RMSD density of the three simulated NS3 structures.** (A) The RMSD of three simulated NS3 "all" amino acid residues throughout the MD simulation compared to the starting structure (unphosphorylated WT at time 0 ns). The WT is shown in "black," S137 is in "light blue," and T189 is in "red." (B) The RMSD density plots of each of three simulated NS3 "all" amino acid residues throughout the MD simulation compared to the starting structure (unphosphorylated WT at time 0 ns). The mean of all RMSD values = 5.6 is shown by the black vertical line. (C) The RMSD of three simulated NS3 amino acid residues (49 – 94) throughout the MD simulation compared to the starting structure (unphosphorylated WT at time 0 ns). (D) The RMSD density plots of each of three simulated NS3 amino acid residues (49 – 94) throughout the MD simulation compared to the starting structure (unphosphorylated WT at time 0 ns). The mean of all RMSD values = 5 is shown by the black vertical line.

To further explore the difference between NS3 in the unphosphorylated state (WT) and phosphorylated at residue S137 or residue T189, a principal component analysis was performed on the cartesian coordinates of the amino acid residues (Fig. 4). There are significant differences between the three structures in PC1 (Fig. 4A). NS3 phosphorylated at S137 is different from unphosphorylated (WT) and phosphorylated at T189 in PC1 for residues 49-94 (Fig. 4B). Fig. 4C shows that the differences in 566-585 between the three states display more overlap in the distributions.

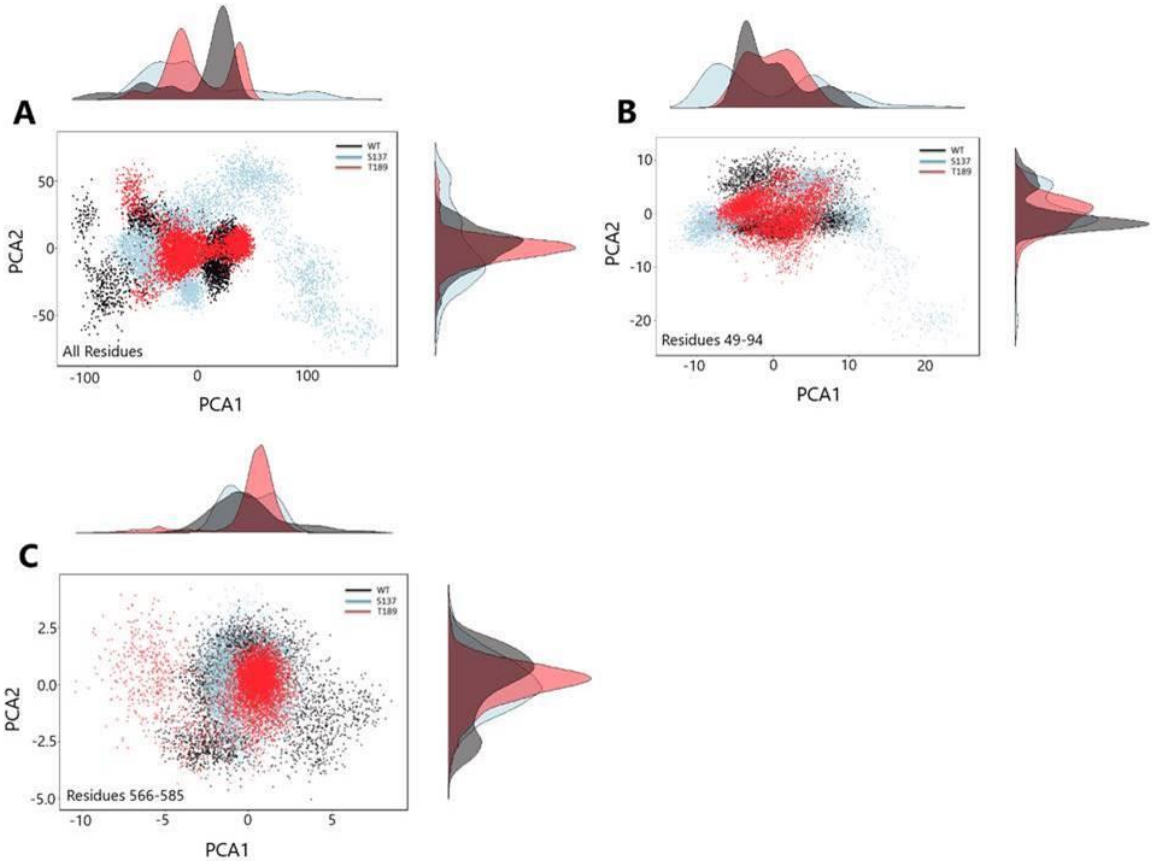


**Fig. 4 Principal Component Analysis (PCA) of the cartesian coordinates through the simulation for the three simulated NS3 structures.** (A) Principal Component 1 vs. Principal Component 2 of three simulated NS3 "all" amino acid residues throughout the MD simulation compared to the starting structure (unphosphorylated WT at time 0 ns). The WT is shown in "black," S137 is in "light blue," and T189 is in "red." (B) Principal Component 1 vs. Principal Component 2 of three simulated NS3 amino acid residues (49

– 94) throughout the MD simulation compared to the starting structure (unphosphorylated WT at time 0 ns). The WT is shown in "black," S137 is in "light blue," and T189 is in "red." (C) Principal Component 1 vs. Principal Component 2 of three simulated NS3 amino acid residues (566 – 585) throughout the MD simulation compared to the starting structure (unphosphorylated WT at time 0 ns). The WT is shown in "black," S137 is in "light blue," and T189 is in "red."

**Table 1 –** *ANCOVA of The Simulated Structures RMSD (all residues) After Adjusting for The Time Steps*

| *Effect* | *DFn* | *DFd* | *F* | *ges* | *p* |
|---|---|---|---|---|---|
| Time Step | 4795 | 9590 | 4.443 | 0.69 | <0.0001 |
| Category | 2 | 9590 | 59671.861 | 0.926 | <0.0001 |

*DFn* = degrees of freedom in the numerator, *DFd* = degrees of freedom in the denominator, *F* = the F-distribution (F-test), *ges* = is the generalized effect size.

**Table 2 –** *Estimated Marginal Means (emmean) Pairwise Comparisons of The Simulated Structures RMSD (all residues)*

| | | | | RMSD emmean Comparisons[1] | | |
|---|---|---|---|---|---|---|
| Category | *emmean* | *SE* | *DF* | S137 | T189 | WT |
| S137 | 7.785 | 0.012 | 14385 | NA | <0.0001 | <0.0001 |
| T189 | 3.871 | 0.012 | 14385 | <0.0001 | NA | <0.0001 |
| WT | 5.396 | 0.012 | 14385 | <0.0001 | <0.0001 | NA |

[1]Bonferroni adjusted p.values. *SE* = Standard Error, *DF* = Degrees of Freedom.

**Table 3 –** *ANCOVA of The Simulated Structures RMSD (residues 49 – 94) After Adjusting for The Time Steps*

| *Effect* | *DFn* | *DFd* | *F* | *ges* | *p* |
|---|---|---|---|---|---|
| Time Step | 4795 | 9590 | 0.843 | 0.297 | 1 |
| Category | 2 | 9590 | 1296396.55 | 0.996 | <0.0001 |

*DFn* = degrees of freedom in the numerator, *DFd* = degrees of freedom in the denominator, *F* = the F-distribution (F-test), *ges* = is the generalized effect size.

**Table 4 –** *Estimated Marginal Means (emmean) Pairwise Comparisons of The Simulated Structures RMSD (residues 49 – 94)*

| | | | | RMSD emmean Comparisons[1] | | |
|---|---|---|---|---|---|---|
| Category | *emmean* | *SE* | *DF* | S137 | T189 | WT |
| S137 | 11.002 | 0.0045 | 14385 | NA | <0.0001 | <0.0001 |
| T189 | 1.908 | 0.0045 | 14385 | <0.0001 | NA | <0.0001 |
| WT | 1.733 | 0.0045 | 14385 | <0.0001 | <0.0001 | NA |

[1]Bonferroni adjusted p.values. *SE* = Standard Error, *DF* = Degrees of Freedom.

### 3.3. *Protein movement changes with phosphorylation*

The RMSF measures the mobility of the protein backbone amino acid residues. We calculated RMSF for three MD simulated structures (unphosphorylated WT at time 100 ns, S137 at time 100 ns, and T189 at time 100 ns) throughout the simulation compared to the starting confirmation (unphosphorylated WT at time 0 ns) (Fig. 5). S137 had more substantial fluctuations of all residues (more prominent in resides 50 to 120) than WT and T189 (Fig. 5A). A closer look for RMSF in residues (49-94) showed an apparent increase in RMSF value in S137 residues (40-50) compared to WT and T189 (Fig. 5B). S137 residues (566-586) showed a pattern close to WT and T189 (Fig. 5C).

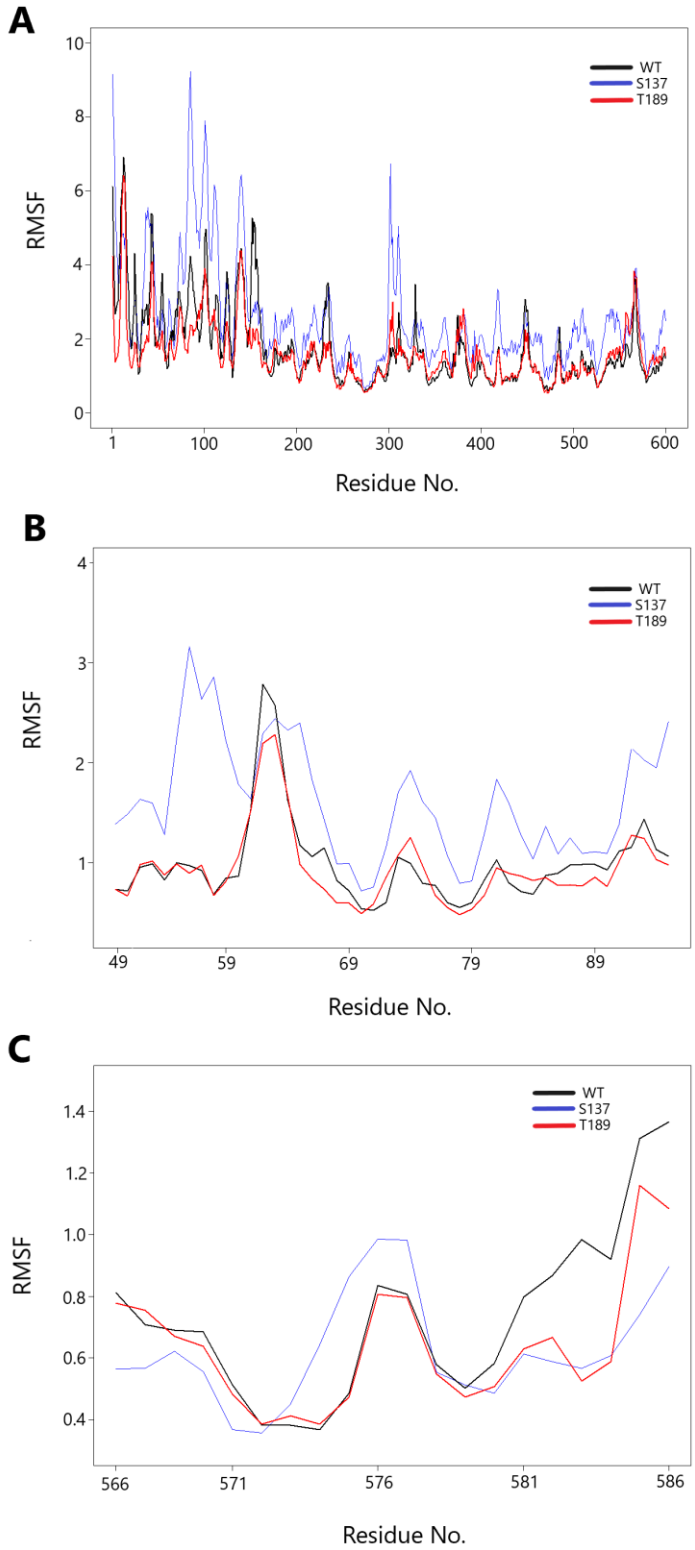
A
RMSF
Residue No.
WT
S137
T189
B
RMSF
Residue No.
WT
S137
T189
C
RMSF
Residue No.
WT
S137
T189

**Fig. 5 Root Mean Square Fluctuation (RMSF) Vs. MD simulation the three simulated NS3 structures.** Phosphorylation at serine 137 (S137) increases NS3 protein all residues fluctuation. (A)The RMSF of three simulated NS3 "all" amino acid residues throughout the MD simulation compared to the starting structure (unphosphorylated WT at time 0 ns). The WT is shown in "black," S137 is in "blue," and T189 is in "red." (B) The RMSF of three simulated NS3 (residues 49–95) shows an evident rise in RMSF value in S137 residues (40-50) compared to WT and T189. (C) The RMSF of three simulated NS3 (residues 566-586) shows a close pattern of the three simulated structures.

### 3.4. *Hydrophobicity of the NS3-NS5 contact site increases with phosphorylation*

Computing solvent accessible surface area (SASA) is one of the widely accepted methods to measure the changes in the accessibility of protein to solvent. SASA typically accounts for the free surface area of water molecules within a radius of 1.4 Å. In this paper, The SASA of MD simulated structures (wild type WT, S137, and T189 during the simulation time 100 ns) was calculated. The higher the SASA score, the more hydrophilic the residue, suggesting that the atoms are exposed more to water. This SASA may indicate an interaction site with other proteins, such as NS5 or a protein kinase. Fig. 6A shows the SASA score for residues 49-95 for the WT (Black), S137 (Blue), and T189 (Red) at simulation time 100 ns. Fig. 6B shows the differences in the SASA scores between S137 and WT (blue) and T189 and WT (red) normalized with respect to the WT score. The differences between S137 and WT are larger than the differences between T189 and WT, most notably between residues 50-58 and 77-85. Fig. 6C shows the SASA scores for residues 566-585. Unlike S137, the SASA score differences between S137 and WT compared to the SASA differences between T189 and WT for residues 566-585 are very small, if any (Fig. 6D). These results are consistent with the MD trajectories RMSD and RMSF, consistent with earlier work showing changes of the catalytic site for NS3 (49-95) and less change to the interface for the NS3-NS5 interaction [44].

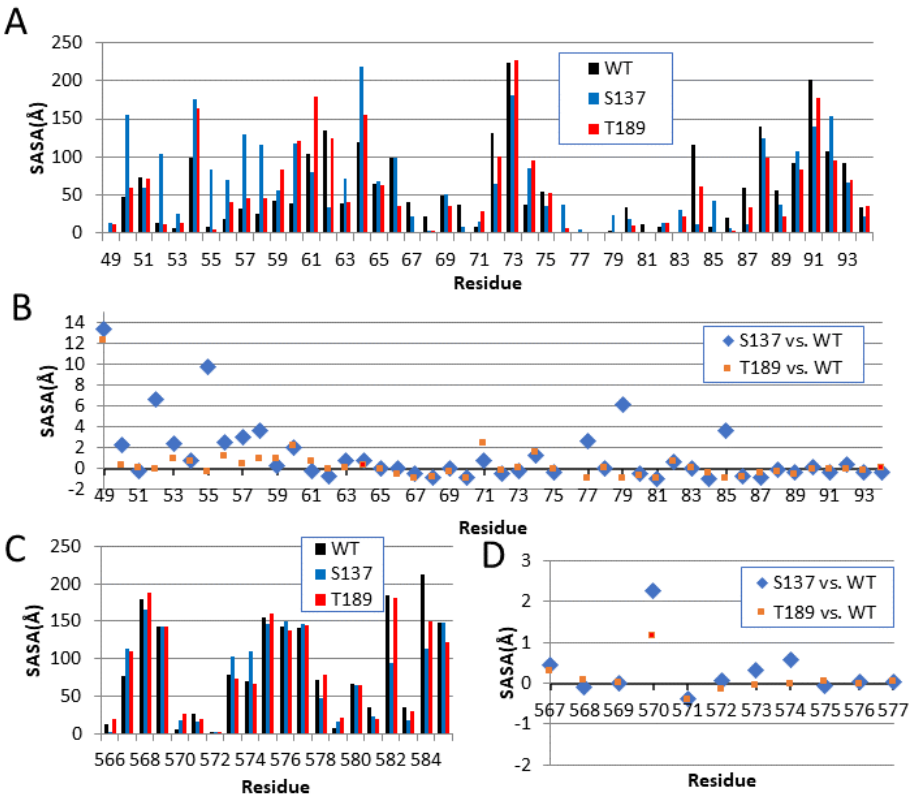


**Fig. 6 The Solvent Accessible Surface Area (SASA) of the two "100 ns" MD simulated structures (unphosphorylated WT at time 100 ns, S137, and T189 at time 100 ns).** Phosphorylation of S137 increases the solvent accessibility at many of the residues. (A) SASA scores for residues 49-95 of WT (Black), S137 (Blue), and T189 (Red) at 100 ns simulation time, (B) The difference in SASA score for residues 49-95 (S137 vs. WT in Blue) and (T189 vs. WT in Red) normalized with respect to WT value. (C) SASA scores for residues 566-585 at 100 ns simulation time, WT (Black), S137 (blue), and T189 (Red). (D) The normalized difference in SASA score for residues 566-585 (S137 vs. WT in Blue) and (T189 vs. WT in Red).

### 3.5. *Phosphorylation induced site-specific structural changes*

Detection of increased negative-strand RNA synthesis by real-time RT-PCR for the NS3 N570A mutant suggests that NS3-NS5 interaction plays a vital role in the balanced synthesis of positive negative-strand RNA for robust viral replication [56]. In particular, the 50 C-terminal amino acid residues are essential for this interaction. After 100 ns of simulation, the phosphorylation effect shows a clear separation of WT residues (566-585) from the same residues in S137 and T189 (Fig. 7). This is consistent with the simulation results shown in Fig. 5. This raises the possibility that the phosphorylation of residues S137 in NS3 might disrupt the NS3-NS5 interaction through changes in the structure at residues 566–585.

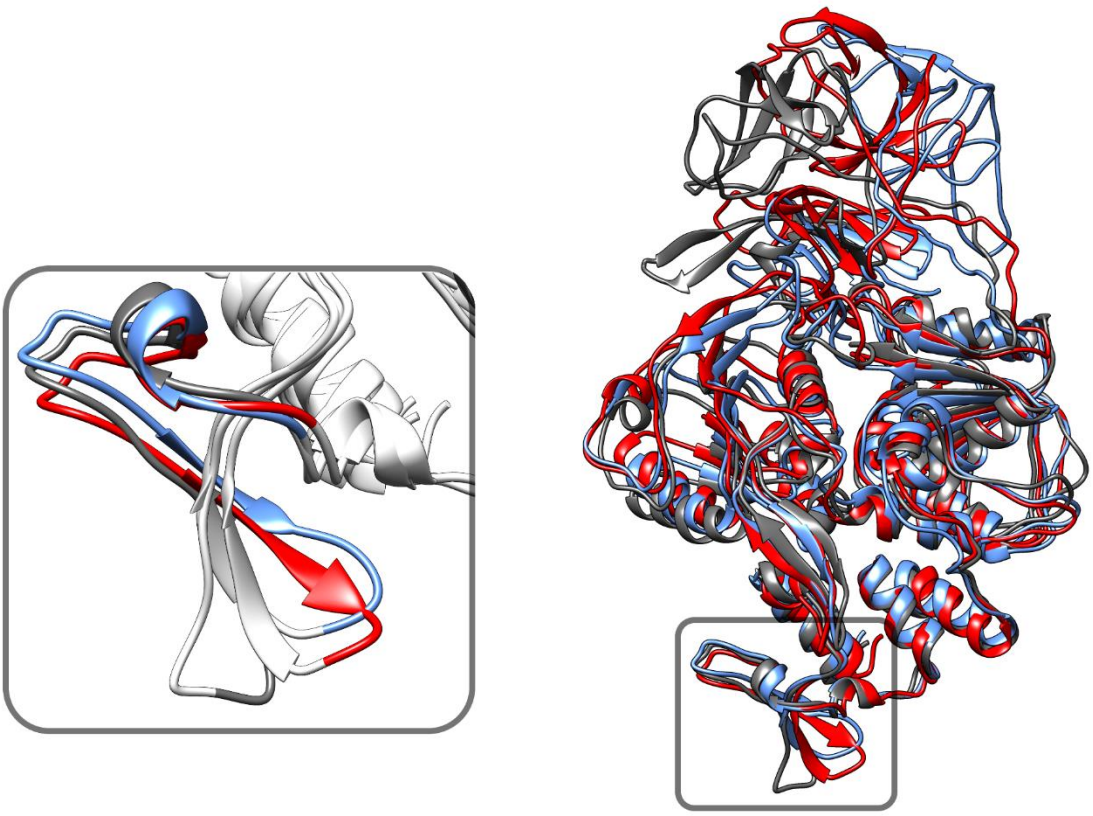

**Fig. 7 Site-specific changes in NS3 structure with phosphorylation.** The C-terminal amino acid residues are essential for the interaction of NS3 with NS5. The three simulated structures at time 100 ns. WT residues 566-585 (inside the box) shows an apparent separation from S137 and T189.

### 3.6. *Docking Analysis of NS3-NS5 Interaction*

We used ClusPro2 (protein-protein blind docking tool) To assess the NS3 specific-site phosphorylation on the NS3-NS5 macromolecule stability based on the docking energy. Lower energy indicates a more stable interaction. We docked three simulated structures (unphosphorylated WT at time 100 ns, T189 at time 100 ns, and S137 at time 100 ns) against the NS5. ClusPro uses the following equation to calculate the binding energy:

$$E = 0.40Erep + -0.40Eatt + 600Eelec + 1.00EDARS \qquad (1)$$

The S137-NS5 complex had the lowest docking energy (-1204.2 Kcal/mol) compared to both T187-NS5 (-960.8 Kcal/mol) and WT-NS5 (-1045.0 Kcal/mol) (Table.5). Phosphorylation at T189 decreased the binding affinity to NS5 compared to WT. The docking results may indicate that NS3 serine 137 (S137) phosphorylation is stabilizing the NS3-NS5 complex.

**Table 5** *NS3-NS5 docking energies.*

| ID | *Weighted Score Lowest energy*[a] |
|---|---|

| | |
|---|---|
| WT-NS5 | -1023.5 Kcal/mol |
| T189-NS5 | -1089.6 Kcal/mol |
| S137-NS5 | -1263.6 Kcal/mol |

*a* = ClusPro docking results (protein-protein blind docking). The balanced form of the equation has been used.

This section may be divided by subheadings. It should provide a concise and precise description of the experimental results, their interpretation, as well as the experimental conclusions that can be drawn.

### 3.7. *Interactions of NS3 with Quercetin*

Quercetin is a plant flavonoid that experimentally inhibits Dengue replication and binds to NS3. The flavonoid Quercetin has been reported to significantly reduce dengue DENV serotype two levels by 67% [57]. Studies have measured Quercetin's binding kinetics to NS3, estimating a $K_D$ of 20 μM [14]. Computational studies using molecular docking strongly suggested Quercetin's binding site to NS2B-NS3; however, the mechanism of viral inhibition is still unknown [13,14].

Auto-dock Vina yielded 10 poses of Quercetin against the protease part of the Dengue virus NS3 Protease-Helicase. The site of docking is similar to those found in previous studies (13, 14). The binding free energy of these poses is ranging from -6.4 to -7.4 kcal/mol. The pose with the lowest energy is shown in (Fig. 8). Hydrogen bonds have been added to Dengue virus NS3 Protease-Helicase before and after Quercetin docking. Two hydrogen bonds connect Quercetin to the protease part of the Dengue virus, one bond with GLN 167 and THR 166. The Quercetin position physically occludes access to S137, suggesting a possible mechanism where Quercetin blocks the phosphorylation of NS3 at 137. This keeps the binding affinity between NS3 and NS5 at a lower level allowing their dissociation, which interferes with viral replication.

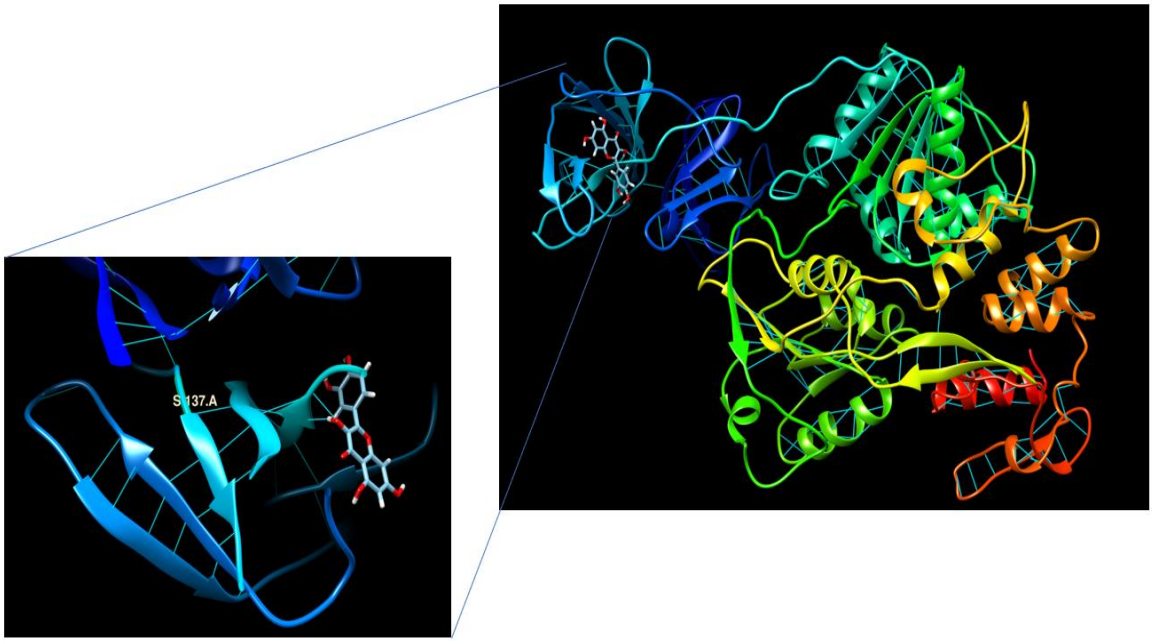

**Fig. 8 Docking of Quercetin with NS3.** Auto-dock of Quercetin against the protease part of the Dengue virus shows that Quercetin binds very close to the S137 site occluding its access.

## 4. Discussion

The disruption of NS3-NS5 interaction results in the transport of NS5 to the nucleus, which decreases viral replication, suggesting that S137 phosphorylation aids in dengue (and flavivirus replication) [11]. Among the MAPKs, there are the JNK and p38 kinases, whose pathways are activated during DENV infection in macrophages. Previous experimental studies have found that phosphorylation by JNK, ERK1/2, and P38 MAPK is activated during Dengue infection and that the inhibitors of JNK and p38 pathways reduce the viral activity [58,59].

Analyses using GPS 3.0, NetPhos 3.1, and Scansite 3 revealed many potential candidate phosphorylation sites on NS3 for several kinases. Candidate sited were screen based on conservation across Dengue Virus sequences based on previous studies that reported that phosphoproteins are subject to more conservation in evolution than their non-phosphorylated proteins [51,52]. This combined *in silico* prediction ranked S137 and T189 as the top two candidates phosphorylated sites. Phosphorylation at NS3 S137 was predicted for MAPK, GSK3, CDK1, and JNK2. Experimental studies have shown that activation of JNK enhances Dengue infection, supporting this prediction [58,59].

In our study, we explore how phosphorylation of NS3 affects the NS3-NS5 complex stability. The two most conserved phosphorylation sites, based on computational prediction, are NS3 serine 137 (S137) and NS3 threonine 189 (T189). MD simulations show that NS3 phosphorylation at S137 leads to a significant conformational change in the NS3 catalytic domain at residues 49 - 94 compared to unphosphorylated NS3 WT and NS3 phosphorylated at T189. This is shown by the RMSD calculation, the RMSF, and SASA scores from the simulations. Furthermore, docking studies show that NS3 phosphorylation at S137 increased the binding affinity between NS3 and NS5 to a much greater extent than NS3 phosphorylation at T189.

The NS3 domain containing S137 is a crucial functionally conserved region in the flavivirus family [24]. Protein homology models have suggested that this residue is involved in the "catalytic triad" (His-Asp-Ser135) that is conserved in all flaviviruses and is necessary for viral replication [24]. Site-directed mutagenesis of NS3, which converting Ser to and Ala at residue 135 in yellow fever virus (equivalent to S137 in Dengue virus), abolished the viral replication [60]. Computational studies have explored the catalytic triad as a drug-target in screens for potential substrates [3,61-64]. However, these studies could not link a potential drug candidate to an experimentally observed reduction in viral replication [61-64]. The proximity of NS3 S137 to this critical triad site suggests that its phosphorylation is likely to be functionally important. Our work is consistent with earlier work on the active site (catalytic triad) for NS3, which showed high mobility during MD simulation [56]. Furthermore, a mutational study shows that L75A, I77A, and I79A mutants demonstrated inefficient autoproteolysis [65]. In our simulations, the SASA scores for these residues change significantly with phosphorylation as S137, as shown in Table 6.

**Table 6** *Solvent Accessible Surface Area (SASA) score for residues 75, 177, and 179.*

| *Residue* | *WT* | *S137* | *T189* |
|---|---|---|---|
| 75 | 54.42 | 35.07 | 52.11 |
| 177 | 100.35 | 22.45 | 122.17 |
| 179 | 56.54 | 100.64 | 82.61 |

Several plant flavonoids have been shown to display antiviral activity against viruses in the flavivirus family, including the Dengue virus. These include Quercetin,

Agathisflavone, and Myricetin, which have been shown to bind NS3 at the same site [13,14]. Quercetin binds with the highest affinity with a disassociation constant of 20 Micrometre (μM). Docking simulations performed in the current study predict that Quercetin binds NS3 to occlude access to the S137 phosphorylation site. Quercetin JNK inhibition is used in treating cardiovascular diseases related to vascular smooth muscle cells (VSMC) growth and apoptosis [66]. In essence, this provides a molecular target for Dengue virus inhibition and suggests that these flavonoids are all acting at this site. The *in silico* findings presented here set up future experimental studies to explore this hypothesis and advance the current understanding of Dengue infection and may provide ways to inhibit viral replication. Future studies will also include experimental verification that flavonoids such as Quercetin act at this site to prevent phosphorylation at residue S137. Quercetin is predicted to bind this site with low affinity to be a suitable drug. Therefore, other compounds that bind this site would need to be developed. Such studies would be followed by optimizing lead compounds, possibly similar to Quercetin, Agathisflavone, and Myricetin, since having the molecular target and structure would allow a pharmacophore model to be developed.

## 5. Conclusions

This section is not mandatory but can be added to the manuscript if the discussion is unusually long or complex. To our knowledge, this is the first study that examined the structural effects of NS3 specific amino acid residue phosphorylation on protein structure and its impact on NS3 and NS5 interaction, and consequently, on DENV viral replication. In summary, the computational analysis and molecular simulations presented in the study make four predictions. First, we predict that the phosphorylation of NS3 at S137 strengthens its association with NS5. Second, these studies predict that JNK phosphorylates NS3 as the S137 site. Third, the study predicts that Quercetin and other plant flavonoids inhibit viral replication by binding near this site to obstruct access to S137. Fourth, given the high degree of homology of this region of NS3 in the flavivirus family, this presents a common potential mechanism across members in this family, except perhaps Hepatitis C virus, which lacks S137 (Supplemental Fig S2 and S3). While these predictions are consistent with existing experimental studies, future work is needed to test these hypotheses.

## 6. Patents

None.

**Supplementary Materials:** The following are available online at www.mdpi.com/xxx/s1, Figure S1: title, Table S1: title, Video S1: title.

**Author Contributions:** LA and SJ conceptualized and initiated this work. LA conducted and analyzed molecular dynamics simulations, AU and FA helped with molecular dynamics simulations. FA helped with R based analysis, statistical testing, and docking. LA wrote the original draft. All authors contributed to the discussion, the analysis of data, and the final draft of the paper.

**Funding:** Please add: This work was supported by King Abdullah International Medical Research Center (KAIMRC) (LA), King Fahad Specialist Hospital -Dammam (KFSH-D) (FA). National Institutes of Health (NIH) supported this research (grant no. 5R01HL105239 and 5U01HL116321) (MSJ & AU).

**Institutional Review Board Statement:** Not applicable.

**Informed Consent Statement:** Not applicable.

**Data Availability Statement:** Data will be deposited into the Mason Archival Repository Service (MARS) at http://mars.gmu.edu upon manuscript acceptance.

**Acknowledgments:** The authors would like to thank Robert Lipsky (George Mason University and INOVA Hospital, Fairfax VA, USA) and Habib Bokhari (COMSATS University, Islamabad Pakistan) for their helpful comments during this work. The authors would like to thank Mohamed A. Hussein (formerly Chairman, Department Biostatistics and Bioinformatics, King Abdullah International Medical Research Center National Guard Riyadh Saudi Arabia) for his support. The authors are grateful to Dmitri Klimov (School of Systems Biology, George Mason University, Fairfax, VA) for his helpful comments on Molecular dynamics simulations.

**Conflicts of Interest:** The authors declare no conflict of interest. The funders had no role in the design of the study; in the collection, analyses, or interpretation of data; in the writing of the manuscript, or in the decision to publish the results.

## Appendix A

The appendix is an optional section that can contain details and data supplemental to the main text—for example, explanations of experimental details that would disrupt the flow of the main text but nonetheless remain crucial to understanding and reproducing the research shown; figures of replicates for experiments of which representative data is shown in the main text can be added here if brief, or as Supplementary data. Mathematical proofs of results not central to the paper can be added as an appendix.

**Table A1 –** The top 20 predicted phosphorylation sites.

| GPS | | | Netphos | | | ScanSite | | |
|---|---|---|---|---|---|---|---|---|
| **Kinase** | **Position** | **Score** | **Kinase** | **Postion** | **Score** | **Kinase** | **Position** | **Score** |
| *MAPK* | *9* | *23.1* | *cdk5* | *9* | *0.59* | *CDK5* | *9* | *0.64* |
| SRC | 23 | 10.1 | SRC | 23 | 0.49 | PRKCZ(PKC) | 45 | 0.52 |
| PIKK | 34 | 9.57 | PKC | 122 | 0.55 | PRKCE(PKC) | 68 | 0.49 |
| PKC | 45 | 9.56 | *cdk5* | *131* | *0.68* | *GSK3A* | *131* | *0.56* |
| PIKK | 127 | 9.45 | ***GSK3*** | ***137*** | ***0.49*** | MAPK3 | 135 | 0.61 |
| *MAPK* | *131* | *28* | PKC | 163 | 0.53 | ***CDK1*** | ***137*** | ***0.6*** |
| MAPK | 134 | 11.3 | PKC | 168 | 0.68 | PRKDC(PIKK) | 171 | 0.58 |
| ***MAPK*** | ***137*** | ***28.8*** | ***PKB(AKT)*** | ***189*** | ***0.73*** | ***CAMK2G*** | ***189*** | ***0.53*** |
| ***AKT*** | ***189*** | ***10.9*** | PKC | 200 | 0.73 | CDK1 | 244 | 0.63 |
| MAPK | 244 | 25.7 | PKC | 218 | 0.71 | AKT1 | 271 | 0.69 |
| MAPK | 271 | 31.4 | cdk5 | 244 | 0.65 | PRKCD(PKC) | 293 | 0.49 |
| *MAPK* | *317* | *28.3* | PKC | 266 | 0.85 | *MAPK3* | *317* | *0.63* |
| PKC | 364 | 9.68 | cdk5 | 271 | 0.65 | GSK3A | 321 | 0.58 |
| PKC | 389 | 10.7 | PKC | 293 | 0.53 | CAMK2G | 358 | 0.6 |
| PKC | 453 | 9.95 | PKC | 301 | 0.67 | PRKCA(PKC) | 364 | 0.53 |
| SRC | 472 | 11.9 | *cdk5* | *317* | *0.65* | CAMK2G | 386 | 0.56 |
| MAPK | 500 | 29.9 | PKC | 352 | 0.6 | PRKACG(PKC) | 389 | 0.6 |
| PKC | 507 | 9.59 | PKC | 358 | 0.63 | MAPK3 | 500 | 0.59 |
| SRC | 523 | 10.3 | PKC | 386 | 0.61 | AKT1 | 602 | 0.71 |

**Table A1.** Top 20 phosphorylation site candidates based upon phosphorylation prediction software. Sites identified by all three software are shown in italics. The two most highly conserved sites are shown in bold.

```
                                  Aura|4UON|A                        --------TGAGGPGDSGRPILDNSGKVVAIVLGGANEGARTALSV--------------   140
                                  Chikungunya|3J2W|I                 --------TGAGKPGDSGRPIFDNKGRVVAIVLGGANEGARTALSV--------------   130
                                  Barmah                             --------TGSGKPGDSGRPIFDNTGKVVAIVLGGANEGARTALSV--------------   234
                                  Hep_C,                             RGALLSPRPISTLKGSSGGPVLCPRGHVVGLFRAAVCSRGVAKSIDFIPVETLDVVTRSP   200
                                  Yellow_fever                       -GGEIGAVALDYPSGTSGSPIVNRNGEVIGLYGNGILVGDNSFVSAISQTEVKE---EGK   1662
                                  Dengue_2|2FOM|B                    -TGTIGAVSLDFSPGTSGSPIVDKKGKVVGLYGNGVVTRSGAYVSAIANTEKSI---E-D   174
                                  Dengue_3,                          -TGEIGAIALDFKPGTSGSPIINREGKVVGLYGNGVVTKNGGYVSGIAQTNAEP---DGP   184
flavivirus                        Dengue_virus|2WZQ|A                -TGEIGAVTLDFKPGTSGSPIINKKGKVIGLYGNGVVTKSGDYVSAITQAERIG---EGP   175
                                  Dengue_4|2VBC|A                    -TGEIGAVTLDFKPGTSGSPIINKKGKVIGLYGNGVVTKSGDYVSAITQAERIG---E-P   174
                                  Zika|5YOD|B                        -DGDIGAVALDYPAGTSGSPILDKSGRVIGLYGNGVVIKNGSYVSAITQGKREE---ETP   176
                                  West_Nile                          -EGEIGAVTLDFPTGTSGSPIVDKNGDVIGLYGNGVIMPNGSYISAIVQGERMD---EPI   174
                                  Murray_valley_encephalitis|2WV9|A  -HGEIGAVSLDYPIGTSGSPIVNSNGEIIGLYGNGVILGNGAYVSAIVQGERVE---EPV   229
                                  Japanese_encephalitis|4R8T|B       -LGEVGAVSLDYPRGTSGSPILDSNGDIIGLYGNGVELGD-------------------   141
                                                                                 * **↑*:.   * ::.:   .
                                                                                     S137
```

**Fig. A2 Multiple sequence Alignment of *Flavivirus* family.** Dengue viruses (all four serotypes), hepatitis C virus, yellow fever virus, zika virus, West Nile virus, Murray Valley encephalitis, and Japanese encephalitis are all members of the *Flavivirus* family. Aura virus, Chikungunya virus, and Barmah virus (carried by mosquitoes but not of the *Flavivirus* family) are included for comparison. The *Flavivirus* family shows a high homology degree, especially in the regions flanking S137 indicated by the red arrow.

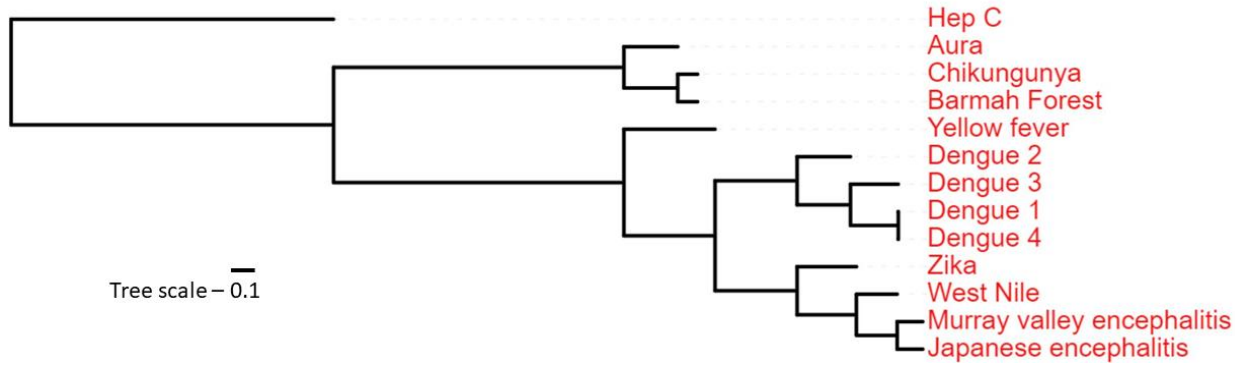


**Fig. A3. Phylogenetic tree for *Flavivirus* family.** Most of the *Flavivirus* family viruses show a close relation, with hepatitis C diverging from the rest. The non-*Flavivirus* family viruses cluster separately.

## References

1. Friedrich, M.J. Asymptomatic People May Contribute to Dengue TransmissionAsymptomatic People May Contribute to Dengue TransmissionGlobal Health. *JAMA* **2016**, *315*, 242-242, doi:10.1001/jama.2015.18460.
2. Beesetti, H.; Khanna, N.; Swaminathan, S. Drugs for dengue: a patent review (2010-2014). *Expert Opin Ther Pat* **2014**, *24*, 1171-1184, doi:10.1517/13543776.2014.967212.

3. Chan, K.W.K.; Watanabe, S.; Jin, J.Y.; Pompon, J.; Teng, D.; Alonso, S.; Vijaykrishna, D.; Halstead, S.B.; Marzinek, J.K.; Bond, P.J., et al. A T164S mutation in the dengue virus NS1 protein is associated with greater disease severity in mice. *Sci Transl Med* **2019**, *11*, doi:10.1126/scitranslmed.aat7726.
4. Murphy, B.R.; Whitehead, S.S. Immune response to dengue virus and prospects for a vaccine. *Annu Rev Immunol* **2011**, *29*, 587-619, doi:10.1146/annurev-immunol-031210-101315.
5. Brady, O.J.; Gething, P.W.; Bhatt, S.; Messina, J.P.; Brownstein, J.S.; Hoen, A.G.; Moyes, C.L.; Farlow, A.W.; Scott, T.W.; Hay, S.I. Refining the global spatial limits of dengue virus transmission by evidence-based consensus. *PLoS Negl Trop Dis* **2012**, *6*, e1760, doi:10.1371/journal.pntd.0001760.
6. Gubler, D.J. Dengue, Urbanization and Globalization: The Unholy Trinity of the 21(st) Century. *Trop Med Health* **2011**, *39*, 3-11, doi:10.2149/tmh.2011-S05.
7. Bidet, K.; Ho, V.; Chu, C.W.; Naim, A.N.H.; Thazin, K.; Chan, K.R.; Low, J.G.H.; Choy, M.M.; Wong, L.H.; Florez de Sessions, P., et al. Mimicking immune signatures of flavivirus infection with targeted adjuvants improves dengue subunit vaccine immunogenicity. *npj Vaccines* **2019**, *4*, 3, doi:10.1038/s41541-019-0119-3.
8. Messina, J.P.; Brady, O.J.; Golding, N.; Kraemer, M.U.G.; Wint, G.R.W.; Ray, S.E.; Pigott, D.M.; Shearer, F.M.; Johnson, K.; Earl, L., et al. The current and future global distribution and population at risk of dengue. *Nature Microbiology* **2019**, 10.1038/s41564-019-0476-8, doi:10.1038/s41564-019-0476-8.
9. Feinberg, M.B.; Ahmed, R. Advancing dengue vaccine development. *Science* **2017**, *358*, 865-866, doi:10.1126/science.aaq0215.
10. Friedrich, M.J. Global Temperature Affects DengueGlobal Temperature Affects DengueGlobal Health. *JAMA* **2018**, *320*, 227-227, doi:10.1001/jama.2018.9737.
11. Freedman, D.; LH, C.; Kozarsky, P. Medical Considerations before International Travel. *N Engl J Med* **2016**, *375*, 247-260.
12. Robinson, M.L.; Durbin, A.P. Dengue vaccines: implications for dengue control. *Curr Opin Infect Dis* **2017**, *30*, 449-454, doi:10.1097/QCO.0000000000000394.
13. Senthilvel, P.; Lavanya, P.; Kumar, K.M.; Swetha, R.; Anitha, P.; Bag, S.; Sarveswari, S.; Vijayakumar, V.; Ramaiah, S.; Anbarasu, A. Flavonoid from Carica papaya inhibits NS2B-NS3 protease and prevents Dengue 2 viral assembly. *Bioinformation* **2013**, *9*, 889-895, doi:10.6026/97320630009889.
14. de Sousa, L.R.; Wu, H.; Nebo, L.; Fernandes, J.B.; da Silva, M.F.; Kiefer, W.; Kanitz, M.; Bodem, J.; Diederich, W.E.; Schirmeister, T., et al. Flavonoids as noncompetitive inhibitors of Dengue virus NS2B-NS3 protease: inhibition kinetics and docking studies. *Bioorg Med Chem* **2015**, *23*, 466-470, doi:10.1016/j.bmc.2014.12.015.
15. Bartholomeusz, A.I.; Wright, P.J. Synthesis of dengue virus RNA in vitro: initiation and the involvement of proteins NS3 and NS5. *Arch Virol* **1993**, *128*, 111-121.
16. Mukhopadhyay, S.; Kuhn, R.J.; Rossmann, M.G. A structural perspective of the flavivirus life cycle. *Nat Rev Microbiol* **2005**, *3*, 13-22, doi:10.1038/nrmicro1067.
17. Limjindaporn, T.; Wongwiwat, W.; Noisakran, S.; Srisawat, C.; Netsawang, J.; Puttikhunt, C.; Kasinrerk, W.; Avirutnan, P.; Thiemmeca, S.; Sriburi, R., et al. Interaction of dengue virus envelope protein with endoplasmic reticulum-resident chaperones facilitates dengue virus production. *Biochem Biophys Res Commun* **2009**, *379*, 196-200, doi:10.1016/j.bbrc.2008.12.070.
18. Reid, D.W.; Campos, R.K.; Child, J.R.; Zheng, T.; Chan, K.W.K.; Bradrick, S.S.; Vasudevan, S.G.; Garcia-Blanco, M.A.; Nicchitta, C.V. Dengue Virus Selectively Annexes Endoplasmic Reticulum-Associated Translation Machinery as a Strategy for Co-opting Host Cell Protein Synthesis. *J Virol* **2018**, *92*, doi:10.1128/JVI.01766-17.
19. Neufeldt, C.J.; Cortese, M.; Acosta, E.G.; Bartenschlager, R. Rewiring cellular networks by members of the Flaviviridae family. *Nature Reviews Microbiology* **2018**, *16*, 125, doi:10.1038/nrmicro.2017.170.

20. Kuno, G.; Chang, G.J.; Tsuchiya, K.R.; Karabatsos, N.; Cropp, C.B. Phylogeny of the genus Flavivirus. *J Virol* **1998**, *72*, 73-83. 638 639
21. Wu, J.; Bera, A.K.; Kuhn, R.J.; Smith, J.L. Structure of the Flavivirus helicase: implications for catalytic activity, protein interactions, and proteolytic processing. *J Virol* **2005**, *79*, 10268-10277, doi:10.1128/JVI.79.16.10268-10277.2005. 640 641
22. Luo, D.; Vasudevan, S.G.; Lescar, J. The flavivirus NS2B-NS3 protease-helicase as a target for antiviral drug development. *Antiviral Res* **2015**, *118*, 148-158, doi:10.1016/j.antiviral.2015.03.014. 642 643
23. Li, Z.; Zhang, J.; Li, H. Chapter 7 - Flavivirus NS2B/NS3 Protease: Structure, Function, and Inhibition. In *Viral Proteases and Their Inhibitors*, Gupta, S., Ed. Academic Press: 2017; pp. 163-188. 644 645
24. Brinkworth, R.I.; Fairlie, D.P.; Leung, D.; Young, P.R. Homology model of the dengue 2 virus NS3 protease: putative interactions with both substrate and NS2B cofactor. *J Gen Virol* **1999**, *80 ( Pt 5)*, 1167-1177, doi:10.1099/0022-1317-80-5-1167. 646 647
25. Papageorgiou, L.; Loukatou, S.; Sofia, K.; Maroulis, D.; Vlachakis, D. An updated evolutionary study of Flaviviridae NS3 helicase and NS5 RNA-dependent RNA polymerase reveals novel invariable motifs as potential pharmacological targets. *Mol Biosyst* **2016**, *12*, 2080-2093, doi:10.1039/c5mb00706b. 648 649 650
26. Kapoor, M.; Zhang, L.; Ramachandra, M.; Kusukawa, J.; Ebner, K.E.; Padmanabhan, R. Association between NS3 and NS5 proteins of dengue virus type 2 in the putative RNA replicase is linked to differential phosphorylation of NS5. *J Biol Chem* **1995**, *270*, 19100-19106, doi:10.1074/jbc.270.32.19100. 651 652 653
27. Natarajan, S. NS3 protease from flavivirus as a target for designing antiviral inhibitors against dengue virus. *Genet Mol Biol* **2010**, *33*, 214-219, doi:10.1590/S1415-47572010000200002. 654 655
28. Alomair, L. Combining Protein Interactions and Functionality Classification in NS3 to Determine Specific Antiviral Targets in Dengue. George Mason University, United States - Virginia, 2017. 656 657
29. Xue, Y.; Liu, Z.; Cao, J.; Ma, Q.; Gao, X.; Wang, Q.; Jin, C.; Zhou, Y.; Wen, L.; Ren, J. GPS 2.1: enhanced prediction of kinase-specific phosphorylation sites with an algorithm of motif length selection. *Protein Eng Des Sel* **2011**, *24*, 255-260, doi:10.1093/protein/gzq094. 658 659 660
30. Blom, N.; Sicheritz-Ponten, T.; Gupta, R.; Gammeltoft, S.; Brunak, S. Prediction of post-translational glycosylation and phosphorylation of proteins from the amino acid sequence. *Proteomics* **2004**, *4*, 1633-1649, doi:10.1002/pmic.200300771. 661 662
31. Obenauer, J.C.; Cantley, L.C.; Yaffe, M.B. Scansite 2.0: Proteome-wide prediction of cell signaling interactions using short sequence motifs. *Nucleic Acids Res* **2003**, *31*, 3635-3641, doi:10.1093/nar/gkg584. 663 664
32. Vlachakis, D.; Bencurova, E.; Papageorgiou, L.; Bhide, M.; Kossida, S. Protein phosphorylation prediction: limitations, merits and pitfalls. *Journal of Molecular Biochemistry* **2015**. 665 666
33. Berman, H.M.; Westbrook, J.; Feng, Z.; Gilliland, G.; Bhat, T.N.; Weissig, H.; Shindyalov, I.N.; Bourne, P.E. The Protein Data Bank. *Nucleic Acids Res* **2000**, *28*, 235-242, doi:10.1093/nar/28.1.235. 667 668
34. Luo, D.; Xu, T.; Hunke, C.; Gruber, G.; Vasudevan, S.G.; Lescar, J. Crystal structure of the NS3 protease-helicase from dengue virus. *J Virol* **2008**, *82*, 173-183, doi:10.1128/JVI.01788-07. 669 670
35. Humphrey, W.; Dalke, A.; Schulten, K. VMD: Visual molecular dynamics. *J Molecular Graphics* **1996**, *14*, 33-38. 671
36. Harrach, M.F.; Drossel, B. Structure and dynamics of TIP3P, TIP4P, and TIP5P water near smooth and atomistic walls of different hydroaffinity. *J Chem Phys* **2014**, *140*, 174501, doi:10.1063/1.4872239. 672 673
37. Phillips, J.C.; Braun, R.; Wang, W.; Gumbart, J.; Tajkhorshid, E.; Villa, E.; Chipot, C.; Skeel, R.D.; Kale, L.; Schulten, K. Scalable molecular dynamics with NAMD. *J Comput Chem* **2005**, *26*, 1781-1802, doi:10.1002/jcc.20289. 674 675
38. Best, R.B.; Zhu, X.; Shim, J.; Lopes, P.E.; Mittal, J.; Feig, M.; Mackerell, A.D., Jr. Optimization of the additive CHARMM all-atom protein force field targeting improved sampling of the backbone phi, psi and side-chain chi(1) and chi(2) dihedral angles. *J Chem Theory Comput* **2012**, *8*, 3257-3273, doi:10.1021/ct300400x. 676 677 678

39. Darden, T.; York, D.; L, P. Particle mesh Ewald: An N·log(N) method for Ewald sums in large systems. *J Chem Phys* **1993**, *98*, 10089-10092. 679 680
40. Grant, B.J.; Rodrigues, A.P.; ElSawy, K.M.; McCammon, J.A.; Caves, L.S. Bio3d: an R package for the comparative analysis of protein structures. *Bioinformatics* **2006**, *22*, 2695-2696, doi:10.1093/bioinformatics/btl461. 681 682
41. Skjaerven, L.; Yao, X.Q.; Scarabelli, G.; Grant, B.J. Integrating protein structural dynamics and evolutionary analysis with Bio3D. *BMC Bioinformatics* **2014**, *15*, 399, doi:10.1186/s12859-014-0399-6. 683 684
42. Haynes, W. Bonferroni Correction. In *Encyclopedia of Systems Biology*, Dubitzky, W., Wolkenhauer, O., Cho, K.-H., Yokota, H., Eds. Springer New York: New York, NY, 2013; 10.1007/978-1-4419-9863-7_1213pp. 154-154. 685 686
43. Vajda, S.; Yueh, C.; Beglov, D.; Bohnuud, T.; Mottarella, S.E.; Xia, B.; Hall, D.R.; Kozakov, D. New additions to the ClusPro server motivated by CAPRI. *Proteins* **2017**, *85*, 435-444, doi:10.1002/prot.25219. 687 688
44. Kozakov, D.; Hall, D.R.; Xia, B.; Porter, K.A.; Padhorny, D.; Yueh, C.; Beglov, D.; Vajda, S. The ClusPro web server for protein-protein docking. *Nat Protoc* **2017**, *12*, 255-278, doi:10.1038/nprot.2016.169. 689 690
45. Kozakov, D.; Beglov, D.; Bohnuud, T.; Mottarella, S.E.; Xia, B.; Hall, D.R.; Vajda, S. How good is automated protein docking? *Proteins* **2013**, *81*, 2159-2166, doi:10.1002/prot.24403. 691 692
46. Trott, O.; Olson, A.J. AutoDock Vina: improving the speed and accuracy of docking with a new scoring function, efficient optimization, and multithreading. *J Comput Chem* **2010**, *31*, 455-461, doi:10.1002/jcc.21334. 693 694
47. Dallakyan, S.; Olson, A.J. Small-molecule library screening by docking with PyRx. *Methods Mol Biol* **2015**, *1263*, 243-250, doi:10.1007/978-1-4939-2269-7_19. 695 696
48. Pettersen, E.F.; Goddard, T.D.; Huang, C.C.; Couch, G.S.; Greenblatt, D.M.; Meng, E.C.; Ferrin, T.E. UCSF Chimera--a visualization system for exploratory research and analysis. *J Comput Chem* **2004**, *25*, 1605-1612, doi:10.1002/jcc.20084. 697 698
49. Alder, B.J.; Wainwright, T.E. Studies in Molecular Dynamics. I. General Method. *J Chem Phys* **959**, *31*, 459-466. 699
50. Wang, Y.; Zheng, Q.C.; Kong, C.P.; Tian, Y.; Zhan, J.; Zhang, J.L.; Zhang, H.X. Heparin makes differences: a molecular dynamics simulation study on the human betaII-tryptase monomer. *Mol Biosyst* **2015**, *11*, 252-261, doi:10.1039/c4mb00381k. 700 701 702
51. Boekhorst, J.; van Breukelen, B.; Heck, A., Jr.; Snel, B. Comparative phosphoproteomics reveals evolutionary and functional conservation of phosphorylation across eukaryotes. *Genome Biol* **2008**, *9*, R144, doi:10.1186/gb-2008-9-10-r144. 703 704
52. Macek, B.; Gnad, F.; Soufi, B.; Kumar, C.; Olsen, J.V.; Mijakovic, I.; Mann, M. Phosphoproteome analysis of E. coli reveals evolutionary conservation of bacterial Ser/Thr/Tyr phosphorylation. *Mol Cell Proteomics* **2008**, *7*, 299-307, doi:10.1074/mcp.M700311-MCP200. 705 706 707
53. Waterhouse, A.M.; Procter, J.B.; Martin, D.M.; Clamp, M.; Barton, G.J. Jalview Version 2--a multiple sequence alignment editor and analysis workbench. *Bioinformatics* **2009**, *25*, 1189-1191, doi:10.1093/bioinformatics/btp033. 708 709
54. Takahashi, H.; Takahashi, C.; Moreland, N.J.; Chang, Y.T.; Sawasaki, T.; Ryo, A.; Vasudevan, S.G.; Suzuki, Y.; Yamamoto, N. Establishment of a robust dengue virus NS3-NS5 binding assay for identification of protein-protein interaction inhibitors. *Antiviral Res* **2012**, *96*, 305-314, doi:10.1016/j.antiviral.2012.09.023. 710 711 712
55. Yang, C.C.; Hu, H.S.; Wu, R.H.; Wu, S.H.; Lee, S.J.; Jiaang, W.T.; Chern, J.H.; Huang, Z.S.; Wu, H.N.; Chang, C.M., et al. A novel dengue virus inhibitor, BP13944, discovered by high-throughput screening with dengue virus replicon cells selects for resistance in the viral NS2B/NS3 protease. *Antimicrob Agents Chemother* **2014**, *58*, 110-119, doi:10.1128/AAC.01281-13. 713 714 715
56. Tay, M.Y.; Saw, W.G.; Zhao, Y.; Chan, K.W.; Singh, D.; Chong, Y.; Forwood, J.K.; Ooi, E.E.; Gruber, G.; Lescar, J., et al. The C-terminal 50 amino acid residues of dengue NS3 protein are important for NS3-NS5 interaction and viral replication. *J Biol Chem* **2015**, *290*, 2379-2394, doi:10.1074/jbc.M114.607341. 716 717 718
57. Zandi, K.; Teoh, B.T.; Sam, S.S.; Wong, P.F.; Mustafa, M.R.; Abubakar, S. Antiviral activity of four types of bioflavonoid against dengue virus type-2. *Virol J* **2011**, *8*, 560, doi:10.1186/1743-422X-8-560. 719 720

58. Ceballos-Olvera, I.; Chavez-Salinas, S.; Medina, F.; Ludert, J.E.; del Angel, R.M. JNK phosphorylation, induced during dengue virus infection, is important for viral infection and requires the presence of cholesterol. *Virology* **2010**, *396*, 30-36, doi:10.1016/j.virol.2009.10.019.
59. Sreekanth, G.P.; Chuncharunee, A.; Cheunsuchon, B.; Noisakran, S.; Yenchitsomanus, P.T.; Limjindaporn, T. JNK1/2 inhibitor reduces dengue virus-induced liver injury. *Antiviral Res* **2017**, *141*, 7-18, doi:10.1016/j.antiviral.2017.02.003.
60. Chambers, T.J.; Weir, R.C.; Grakoui, A.; McCourt, D.W.; Bazan, J.F.; Fletterick, R.J.; Rice, C.M. Evidence that the N-terminal domain of nonstructural protein NS3 from yellow fever virus is a serine protease responsible for site-specific cleavages in the viral polyprotein. *Proc Natl Acad Sci U S A* **1990**, *87*, 8898-8902, doi:10.1073/pnas.87.22.8898.
61. Agnihotri, S.; Narula, R.; Joshi, K.; Rana, S.; Singh, M. In silico modeling of ligand molecule for non structural 3 (NS3) protein target of flaviviruses. *Bioinformation* **2012**, *8*, 123-127, doi:10.6026/97320630008123.
62. Mukhametov, A.; Newhouse, E.I.; Aziz, N.A.; Saito, J.A.; Alam, M. Allosteric pocket of the dengue virus (serotype 2) NS2B/NS3 protease: In silico ligand screening and molecular dynamics studies of inhibition. *J Mol Graph Model* **2014**, *52*, 103-113, doi:10.1016/j.jmgm.2014.06.008.
63. Chen, J.; Jiang, H.; Li, F.; Hu, B.; Wang, Y.; Wang, M.; Wang, J.; Cheng, M. Computational insight into dengue virus NS2B-NS3 protease inhibition: A combined ligand- and structure-based approach. *Comput Biol Chem* **2018**, *77*, 261-271, doi:10.1016/j.compbiolchem.2018.09.010.
64. Velmurugan, D.; Mythily, U.; Rao, K. Design and docking studies of peptide inhibitors as potential antiviral drugs for dengue virus ns2b/ns3 protease. *Protein Pept Lett* **2014**, *21*, 815-827.
65. Niyomrattanakit, P.; Winoyanuwattikun, P.; Chanprapaph, S.; Angsuthanasombat, C.; Panyim, S.; Katzenmeier, G. Identification of Residues in the Dengue Virus Type 2 NS2B Cofactor That Are Critical for NS3 Protease Activation. *Journal of Virology* **2004**, *78*, 13708-13716, doi:10.1128/jvi.78.24.13708-13716.2004.
66. Yoshizumi, M.; Tsuchiya, K.; Kirima, K.; Kyaw, M.; Suzaki, Y.; Tamaki, T. Quercetin inhibits Shc- and phosphatidylinositol 3-kinase-mediated c-Jun N-terminal kinase activation by angiotensin II in cultured rat aortic smooth muscle cells. *Mol Pharmacol* **2001**, *60*, 656-665.

1.